2009

Virtual Circular Array Using Material-Embedded Linear Source Distributions

DoHoon Kwon, *University of Massachusetts - Amherst*

AIP | Applied Physics Letters

Virtual circular array using material-embedded linear source distributions

Do-Hoon Kwon

Citation: Appl. Phys. Lett. **95**, 173503 (2009); doi: 10.1063/1.3257374
View online: http://dx.doi.org/10.1063/1.3257374
View Table of Contents: http://apl.aip.org/resource/1/APPLAB/v95/i17
Published by the American Institute of Physics.

Related Articles

Experimental investigations of the TE11 mode radiation from a relativistic magnetron with diffraction output
Phys. Plasmas 19, 113108 (2012)

Omnidirectional photonic band gap enlarged by one-dimensional ternary unmagnetized plasma photonic crystals based on a new Fibonacci quasiperiodic structure
Phys. Plasmas 19, 112102 (2012)

An oversized X-band transit radiation oscillator
Appl. Phys. Lett. 101, 173504 (2012)

Path derivation for a wave scattered model to estimate height correlation function of rough surfaces
Appl. Phys. Lett. 101, 141601 (2012)

Strong curvature effects in Neumann wave problems
J. Math. Phys. 53, 083507 (2012)

Additional information on Appl. Phys. Lett.

Journal Homepage: http://apl.aip.org/
Journal Information: http://apl.aip.org/about/about_the_journal
Top downloads: http://apl.aip.org/features/most_downloaded
Information for Authors: http://apl.aip.org/authors

ADVERTISEMENT

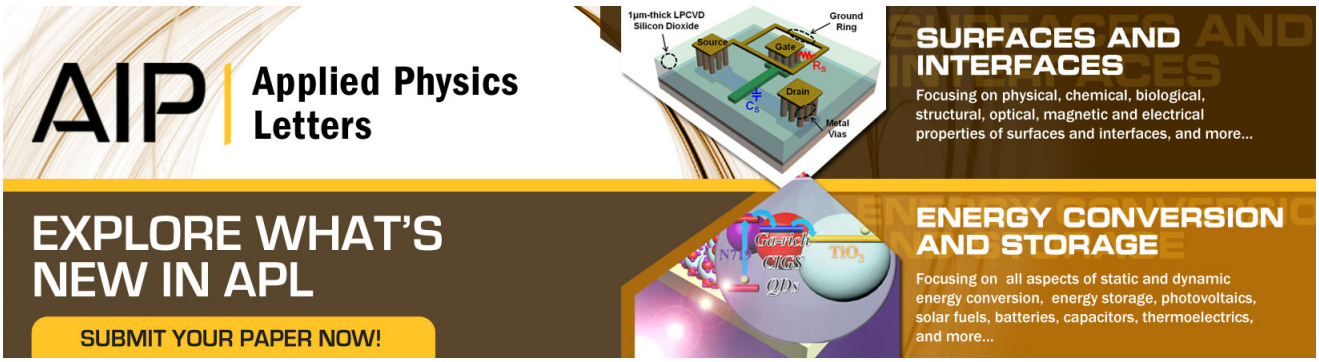

Virtual circular array using material-embedded linear source distributions

Do-Hoon Kwon[a)]
Department of Electrical and Computer Engineering, University of Massachusetts Amherst, Amherst, Massachusetts 01003, USA

(Received 31 July 2009; accepted 8 October 2009; published online 28 October 2009)

Linear arrays of sources embedded inside a thin material slab are designed such that they radiate the same fields as a circular array of radiators in free space in a two-dimensional configuration. The design is based on the coordinate transformation approach, where a circular domain containing a distribution of line sources is transformed into a rectangular slab. The source distribution in the transformed space forms two closely-spaced linear arrays and the resulting material slab is matched along the boundary with free space. Full-wave simulations are performed for verification. © *2009 American Institute of Physics*. [doi:10.1063/1.3257374]

The transformation electromagnetics/optics device design technique, which is based on spatial coordinate transformations and the invariance of Maxwell's equations under such transformations, has lead to numerous device designs that feature unusual wave-material interaction properties. The invisibility cloaks[1–3] are the most prominent examples and various other device designs[4–8] have emerged based on the coordinate transformation approach. It was pointed out in Ref. 9 that the perfect lens[10] can be interpreted as a transformation electromagnetic device that takes advantage of a negative slope in the transformation function, giving rise to negative-index constituent materials. Several additional device designs that take advantage of the negative slope have been reported in the literature.[11–14]

The effects of coordinate transformations on sources were studied and utilized more recently. It was noted that a line sourced embedded within a two-dimensional (2D) cloak appears to be radiating from a different location.[15] A dipole antenna in free space was transformed into a combination of a metamaterial shell and a surface current distribution,[16] and the radiated fields from the two configurations were shown to be the same. The effects of transformations on the current densities and shapes were analyzed in Ref. 17. A circular annular material shell together with a conformal array of sources were designed to radiate like a linear array.[18] Zhang *et al.*[19] demonstrated that a spherical shell can be designed such that an enclosed antenna array can radiate the same field as a virtual array of the same shape in free space that can be physically larger by an arbitrary factor.

In this letter, the source transformation is employed to design a linear array embedded inside a thin rectangular transformation medium that creates the same field as a taller circular array operating in free space. Circular arrays have an advantage of being able to scan at any angle with a constant beamwidth, but they are bulky and nonconformal to flat or smooth platforms. Linear arrays can be conformally installed to planar or smooth surfaces, but their scanning performance degrades significantly at high angles. The thin physical array in this study is smaller than the virtual array contrary to the conformal array design in Ref. 18. The array is planar and low-profile unlike Ref. 19. The thin array can scan in any direction without performance degradation. The effect of material loss on wide-angle scan performance of the array is numerically analyzed.

Consider a circular array of N electric line sources positioned along the circumference of a circle with radius a in free space, as shown in Fig. 1(a) in the original (virtual) (x,y,z) system. The line sources are located at $\mathbf{r}_n = a(\hat{x}\cos\phi_n + \hat{y}\sin\phi_n)$, where $\phi_n = (2n-1)\pi/N$ and they carry electric line currents with complex amplitudes $I_n (n=1,2,\ldots,N)$ flowing in the $+\hat{z}$ direction. It is desired that they are transformed into a linear array of two rows of line sources, as described in Fig. 1(b) in the transformed (physical) (x',y',z') system. We stretch and compress the circular domain only in the $\pm\hat{y}$ directions using the following transformation:

$$x = x', \tag{1}$$

$$y = \begin{cases} \frac{\sqrt{a^2-x^2}}{b} y', & |y'| \le b, \\ \frac{\sqrt{a^2-x^2}-t}{b-t}(y' \mp t) \pm t, & b < |y'| \le t, \\ y', & |y'| > t, \end{cases} \tag{2}$$

$$z = z'. \tag{3}$$

The mapping from y' to y is illustrated in Fig. 2, and y is an odd function of y'. For any given value of x, the range $|y|$

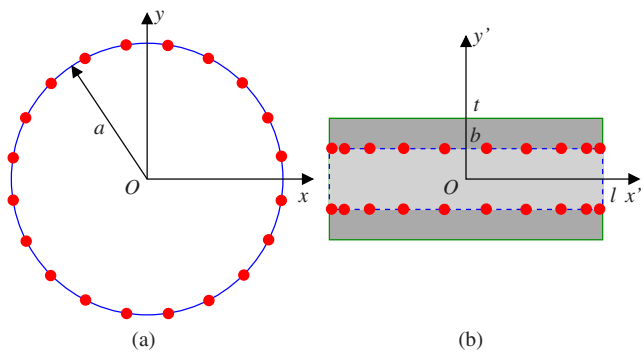

FIG. 1. (Color online) The spatial domains for a linear array design: (a) Original domain. (b) Transformed domain. The transformation moves the original line sources along the circumference of the circle with radius a to the perimeter of a rectangle of dimensions $2l \times 2b$ (red dots). The size of the entire structure in the transformed space is $2l \times 2t$. The gray-shaded regions represent transformation material slabs.

a)Electronic mail: dhkwon@ecs.umass.edu.

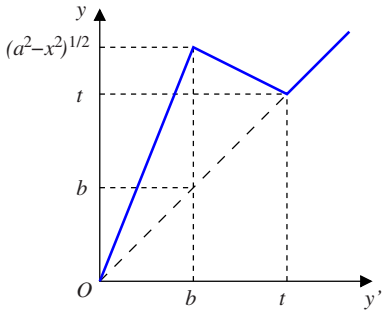

FIG. 2. (Color online) The transformation from y' to y for a given value of x.

$\leq \sqrt{a^2-x^2}$ is compressed into the range $|y'| \leq b$. In addition, the transformation is continuous at $y' = \pm t$. It is observed that $y=y'$ results when $\sqrt{a^2-x^2}=b$. By choosing the horizontal dimension of the transformed space according to $l=\sqrt{a^2-b^2}$, the transformation becomes continuous across the two vertical boundaries at $x' = \pm l$. As a result, the spatial transformation is continuous across all boundary, making the transformation electromagnetic device reflectionless.

Using the Jacobian matrix of the transformation $\mathbf{A} = \partial(x', y', z')/\partial(x, y, z)$, the permittivity and permeability tensor parameters of the transformed domain can be obtained via $\boldsymbol{\epsilon}' = \boldsymbol{\mu}' = \mathbf{A}\mathbf{A}^{\mathrm{T}}/\det(\mathbf{A})$.[3] In the region $|x'| \leq l$, $|y'| \leq b$ [the light gray region in Fig. 1(b)], the relevant material parameters are found to be

$$\mu_{xx} = \epsilon_{zz} = \frac{\sqrt{a^2 - x'^2}}{b}, \tag{4}$$

$$\mu_{xy} = \frac{x'y'}{b\sqrt{a^2 - x'^2}}, \tag{5}$$

$$\mu_{yy} = \frac{b}{\sqrt{a^2 - x'^2}}\left[1 + \frac{x'^2 y'^2}{b^2(a^2 - x'^2)}\right]. \tag{6}$$

The parameters in the region $|x'| \leq l$, $b < |y'| \leq t$ [the dark gray region in Fig. 1(b)] are equal to

$$\mu_{xx} = \epsilon_{zz} = -\frac{\sqrt{a^2 - x'^2} - t}{t - b}, \tag{7}$$

$$\mu_{xy} = -\frac{x'(y' \mp t)}{(t - b)\sqrt{a^2 - x'^2}}, \tag{8}$$

$$\mu_{yy} = -\frac{t - b}{\sqrt{a^2 - x'^2} - t}\left[1 + \frac{x'^2(y' \mp t)^2}{(t - b)^2(a^2 - x'^2)}\right], \tag{9}$$

for $y' > 0$ and $y' < 0$, respectively. It can be seen from Eqs. (7)–(9) that a negative-index material fills the range $|x'| < \sqrt{a^2 - t^2}$ and a positive-index material occupies the range $\sqrt{a^2-t^2} < |x'| \leq l$. At $|x'| = \sqrt{a^2-t^2}$, μ_{yy} possesses a singularity. Finally, removing the primes in Eqs. (4)–(9) gives the material parameters in the familiar (x, y, z) system.

Since the original space contains sources, they are subject to the transformation as well as the space. In the case of line currents, only the current locations are translated without any modifications to current amplitudes.[16] Although the line currents are located on the boundary of the original domain, we can treat them as internal points by considering the circular domain to have the radius $a+\Delta a$ and letting $\Delta a \to 0^+$. If we let $\Delta a \to 0^-$, the locations of the line sources will be unaffected by the transformation, which is not a case of interest. According to Eqs. (1)–(3), the positions of the new line sources are given by $\mathbf{r}'_n = \hat{x}a \cos \phi_n + \hat{y}b \sin \phi_n / |\sin \phi_n|$ $(n = 1, 2, \ldots, N)$. The original and the transformed line source locations are indicated by red dots in Fig. 1.

The circular array in free space is now transformed into a linear array embedded inside a transformation material. The linear array should radiate and receive exactly the same field as the circular array. The validity is numerically tested and verified using a commercial package COMSOL Multiphysics. Consider a 20-element $(N=20)$ circular array at 3 GHz $(\lambda = 0.1$ m) with $a = 10\lambda/2\pi = 0.1592$ m. The distance between neighboring sources is approximately 0.5λ. Let the line currents be phased to produce the main beam at the scan angle $\phi = \phi_s$:

$$I_n = e^{-j\mathbf{k}_s \cdot \mathbf{r}_n}; \quad \mathbf{k}_s = k(\hat{x} \cos \phi_s + \hat{y} \sin \phi_s), \tag{10}$$

where $k = 2\pi/\lambda$. Figure 3 compares the $\hat{z}$-directed total electric field distributions for three array configurations. The scan angle of 80° off normal $(\phi_s = 10°)$ is chosen because the scan performance of free space linear arrays significantly degrades at high angles. The electric field distribution for the circular array in free space is shown in Fig. 3(a). When a linear array in Fig. 1(b) is formed without the transformation medium, the distribution in Fig. 3(b) results, showing a wide main beam due to the reduced aperture. In this case, currents were phased according to Eq. (10) with $\mathbf{r}_n$ at the

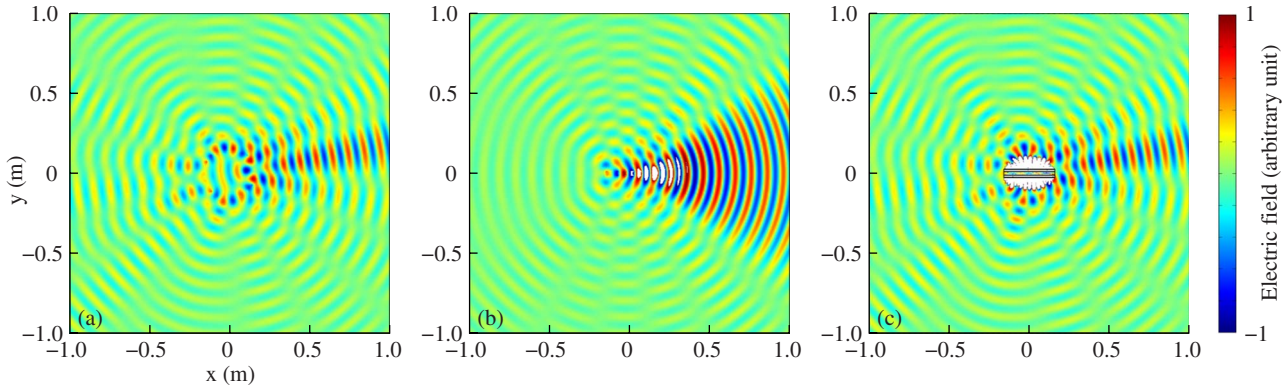

FIG. 3. (Color online) Total electric field distributions for three array configurations for a scan angle of $\phi_s = 10°$: (a) Circular array in free space. (b) Linear array in free space. (c) Linear array embedded in the transformation medium.

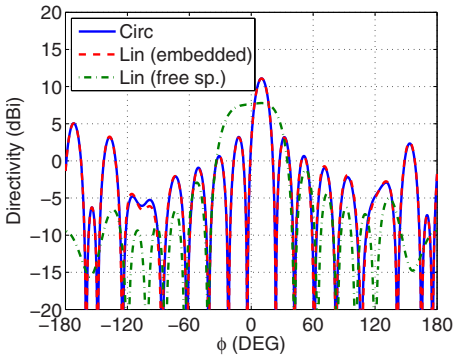

FIG. 4. (Color online) 2D directivity patterns for three array configurations for a scan angle of $\phi_s=10°$.

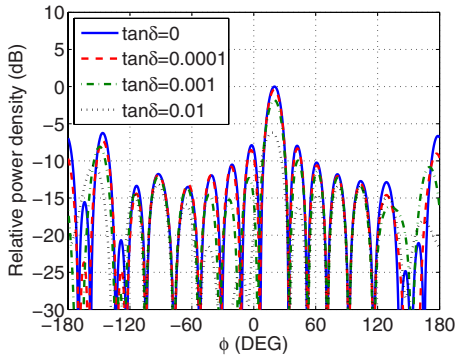

FIG. 5. (Color online) Relative power densities in the far zone for different values of the loss factor. The scan angle is $\phi_s=20°$.

new locations.

The transformation medium-embedded linear array is designed with the parameter values $b=\lambda/8=0.0125$ m and $t=\lambda/4=0.025$ m. The value l is given by $l=0.1587$ m. The circular and the new linear arrays have nearly the same lengths but the height is reduced by a factor of 6.37 for the linear array. When the line sources radiate inside the medium, Fig. 3(c) shows that the generated field is the same as that of the circular array in free space. In Fig. 4, 2D directivities are compared for the three array configurations. The circular array and the material-embedded linear array have the same patterns with the main beam located at $\phi=\phi_s=10°$, whereas the linear array in free space has a broad beam.

Metamaterials are prime candidates for realizing the complex material parameters for the new linear array. Losses in metamaterial realizations may be a limiting factor in practical designs and uses. For a scan angle of $\phi_s=20°$, radiation power densities for different values of the loss factor tan δ relative to the peak density of the lossless case are compared in Fig. 5. Loss was incorporated in the simulations by replacing ϵ_{zz} with $\epsilon_{zz}-j|\epsilon_{zz}|\tan\delta$. Similar modifications were made to other tensor parameters. As loss is increased, the radiated power drops and sidelobe levels increase, but the main beam does not significantly widen in the range $\tan\delta\leq 0.01$. The loss tangent of 0.01 in rf negative-index metamaterials poses a challenge and its realization will be a key to the effectiveness of the design in practice.

The transformation electromagnetics technique was used to design a linear array embedded inside a material such that it performs the same as a larger circular array in free space. The linear array can scan at wide angles including endfire directions without having a broadening main beam.

[1]U. Leonhardt, Science **312**, 1777 (2006).
[2]J. B. Pendry, D. Schurig, and D. R. Smith, Science **312**, 1780 (2006).
[3]D. Schurig, J. B. Pendry, and D. R. Smith, Opt. Express **14**, 9794 (2006).
[4]H. Chen and C. T. Chan, Appl. Phys. Lett. **90**, 241105 (2007).
[5]A. V. Kildishev and E. E. Narimanov, Opt. Lett. **32**, 3432 (2007).
[6]M. Rahm, S. A. Cummer, D. Schurig, J. B. Pendry, and D. R. Smith, Phys. Rev. Lett. **100**, 063903 (2008).
[7]B. Donderici and F. L. Teixeira, IEEE Microw. Wirel. Compon. Lett. **18**, 233 (2008).
[8]D.-H. Kwon and D. H. Werner, New J. Phys. **10**, 115023 (2008).
[9]U. Leonhardt and T. G. Philbin, New J. Phys. **8**, 247 (2006).
[10]J. B. Pendry, Phys. Rev. Lett. **85**, 3966 (2000).
[11]M. Yan, W. Yan, and M. Qiu, Phys. Rev. B **78**, 125113 (2008).
[12]T. Yang, H. Chen, X. Luo, and H. Ma, Opt. Express **16**, 18545 (2008).
[13]H. Chen, X. Luo, H. Ma, and C. T. Chan, Opt. Express **16**, 14603 (2008).
[14]J. Zhang, Y. Luo, H. Chen, J. Huangfu, B.-I. Wu, L. Ran, and J. A. Kong, Opt. Express **17**, 6203 (2009).
[15]F. Zolla, S. Guenneau, A. Nicolet, and J. B. Pendry, Opt. Lett. **32**, 1069 (2007).
[16]Y. Luo, J. Zhang, L. Ran, H. Chen, and J. A. Kong, IEEE Antennas Wireless Propag. Lett. **7**, 509 (2008).
[17]N. Kundtz, D. A. Roberts, J. Allen, S. Cummer, and D. R. Smith, Opt. Express **16**, 21215 (2008).
[18]B.-I. Popa, J. Allen, and S. A. Cummer, Appl. Phys. Lett. **94**, 244102 (2009).
[19]B. Zhang, B.-I. Wu, and H. Chen, *2009 IEEE Antennas and Propagation Society International Symposium* (IEEE, Charleston, 2009).